Hot days induced by precipitation deficits at the global scale

Brigitte Mueller[1] and Sonia I. Seneviratne[1]

Institute for Atmospheric and Climate Science, Eidgenössiche Technische Hochschule (ETH) Zurich, 8092 Zurich, Switzerland

Edited by Mark H. Thiemens, University of California San Diego, La Jolla, CA, and approved June 18, 2012 (received for review March 16, 2012)

Global warming increases the occurrence probability of hot extremes, and improving the predictability of such events is thus becoming of critical importance. Hot extremes have been shown to be induced by surface moisture deficits in some regions. In this study, we assess whether such a relationship holds at the global scale. We find that wide areas of the world display a strong relationship between the number of hot days in the regions' hottest month and preceding precipitation deficits. The occurrence probability of an above-average number of hot days is over 70% after precipitation deficits in most parts of South America as well as the Iberian Peninsula and Eastern Australia, and over 60% in most of North America and Eastern Europe, while it is below 30–40% after wet conditions in these regions. Using quantile regression analyses, we show that the impact of precipitation deficits on the number of hot days is asymmetric, i.e. extreme high numbers of hot days are most strongly influenced. This relationship also applies to the 2011 extreme event in Texas. These findings suggest that effects of soil moisture-temperature coupling are geographically more widespread than commonly assumed.

hot day prediction | soil moisture–temperature coupling | standardized precipitation index | temperature extremes

Warm temperature extremes have significant societal and economic impacts (1). The ability to seasonally predict hot extremes would allow the undertaking of precautionary measures to avoid or reduce their impacts. This is particularly relevant for public health management (2–4). Such predictions are even more important in the view that hot days and heat waves have become more frequent in the second half of the 20th century (5, 6), and that these trends are projected to continue in the future (4, 7–9).

The role of soil moisture anomalies for the occurrence of hot days and the evolution of heat waves in transitional climate regions has been highlighted in several regional studies (10, 11), for example for the 2003 European heat wave (12) and for hot European summers in general (13, 14). Such feedbacks between soil moisture and temperature have also been shown to be relevant for climate change projections (15, 16). In these various studies, soil moisture deficits were mostly found to affect hot extremes through the energy balance: Low soil moisture availability reduces evaporative cooling and increases atmospheric heating from sensible heat flux (10, 14, 17). Nonetheless, indirect feedbacks with cloud cover and dry air advection may also play a role (12, 18, 19).

Here, we explicitly investigate whether information on surface moisture deficits can be used to derive predictive information on the occurrence of hot extremes a few weeks later—and if so, in which regions. In addition to modeling studies (20), previous studies assessed the relation of hot extremes and preceding drought conditions using observational data (14), but to our knowledge, this relationship has never been investigated with observations at the global scale. Moreover, most studies assessing soil moisture-atmosphere coupling in present or future climate (15, 21) focused on boreal summer (June-July-August, JJA), but did not consider months most relevant to the respective regions at the global scale, e.g. austral summer for Southern Hemisphere mid-latitudes. Building upon a recently published study (14), we use here the Standardized Precipitation Index (SPI) (22) as proxy for surface moisture deficits, and we globally assess the impact of these deficits on the occurrence of subsequent hot days in the respective hottest month of each particular year and at each location (see Fig. 1*A*) using correlation analysis and quantile regression (23, 24). While correlation analyses are suitable to study the relationship between two variables' mean states, quantile regression allows to estimate the impact of one variable on the tails of the distribution of another. It should be noted that statistical relationships do not necessarily imply causality, but can be used to assess the coupling between two variables if plausible mechanisms exist (10).

The SPI is the standard deviation of observed precipitation values from the long-term mean after a normalization with the gamma distribution. SPI values lower than −0.8 are usually referred to as moderately to extremely dry, and values higher than 0.8 as moderately to extremely wet. The SPI is calculated from precipitation deficits over a given time period. We consider here the 3-, 6- and 9-month SPI. For all computations, SPI values in the month directly preceding the hottest month of the particular year are considered, which in the case of the 3-month SPI implies, for instance, that April to June precipitation deficits are taken into account for a hottest month occurring in July. The precipitation datasets employed for the calculation of the SPI are gridded, in-situ observations-based datasets (CRU, GPCP, CPC).

Soil moisture deficits can also be estimated from remote sensing (RS) satellite retrievals, such as the European Remote Sensing (ERS), Advanced Microwave Scanning Radiometer for EOS (AMSR-E), or Soil Moisture and Ocean Salinity (SMOS) satellites. Such RS-based datasets provide more direct observations of soil moisture than the SPI, which is based solely on precipitation. However, the SPI has several advantages over satellite-derived soil moisture data: First, it can be calculated over a longer time period than that covered by consistent RS data, which is important to obtain statistically robust results; second, satellite RS data of soil moisture are not fully global (e.g. due to retrieval difficulties over densely vegetated areas (10, 25)); and third, the SPI—contrary to retrievals from RS, which undergo a post-processing—is available in near real time, which is essential for timely forecasting.

Several definitions of hot days exist (9, 26). Here, we define the number of hot days per month (NHD) as the number of days with a maximum temperature exceeding the 90th percentile (sample of warmest decile days). As opposed to e.g. threshold-based indices, percentile-based indices are more comparable across different climatic regions. For the computation of the NHD, we use daily 2-m air temperature from 1979 to 2010 from different

Author contributions: B.M. and S.I.S. designed research; B.M. and S.I.S. performed research; B.M. analyzed data; and B.M. and S.I.S. wrote the paper.

The authors declare no conflict of interest.

This article is a PNAS Direct Submission.

[1]To whom correspondence may be addressed. E-mail: brigitte.mueller@env.ethz.ch or sonia.seneviratne@env.ethz.ch.

This article contains supporting information online at www.pnas.org/lookup/suppl/doi:10.1073/pnas.1204330109/-/DCSupplemental.

datasets: In the main analyses, hot days are calculated from the ECMWF reanalysis ERA-Interim (27), while comparisons to hot days from other reanalyses (CFSR and MERRA) and from an observations-based dataset over Europe are also shown. A time window of five days centered on each day of the 32-year period is considered, i.e. the 90th percentile is calculated from 160 daily values.

Results and Discussion

Global Analyses of Coupling Between Precipitation Deficits and Subsequent Hot Extremes. Correlations between the NHD in the hottest month at each location and the preceding 3-month SPI are displayed in Fig. 1*B*. Several regions exhibit significantly negative correlations, i.e. high (low) NHD following negative (positive) SPI values, and thus a potential for NHD early warning. The correlations of the NHD and the preceding 6- and 9-month SPI are shown in Fig. 1 *C*–*D*. The correlations are smaller for the 6- and 9-month SPI, and regions with significant values are less extended, but the patterns of strong coupling are nearly identical. In the following, as well as for the additional analyses, we will focus on the computations with the 3-month SPI, but the high consistency over all time frames suggests a strong robustness of the results. Note that, given the link between SPI and soil moisture availability, these correlations can also be seen as a measure of coupling strength between the land surface and the atmosphere (10, 21).

The identified regions of strong correlation between surface moisture deficits and temperature extremes are found to be located in most of the Americas (both North and South America), Southern and Eastern Europe, Australia, China, Japan and the southern tip of Africa. Interestingly, these regions are more extended and located in partly different areas than diagnosed in the commonly cited model-based (and boreal-summer) Global Land-Atmosphere Coupling Experiment (GLACE) study (21). However, there are also some common features, mostly the strong coupling found in the Great Plains of North America, and the strong potential predictability found in Europe in the second phase of the GLACE experiment (GLACE-2) (28). In addition, the identified hot spots agree well with the results of another recent model-based study investigating patterns of soil moisture-evapotranspiration coupling computed for all seasons (29) (compare in particular with patterns for JJA and DJF in the mid-latitudes). It should be noted that although the GLACE study (21) is sometimes erroneously interpreted as being a global analysis of land-atmosphere coupling valid for any season or time period, it has various limitations. Most importantly, it is: 1) model-based; 2) limited to the JJA season; 3) limited to the 1994 conditions; and 4) valid for intra-seasonal rather than for interannual variability. The more recent GLACE-2 experiment (28) has similar limitations, except that it has been computed over a longer time period (1986–1995). Our observation-based analysis, by taking into account the respective period of the year where soil moisture is most likely to be limiting in each region, suggests a broader relevance of soil moisture-atmosphere coupling than could be assumed from the well-established GLACE study. Note that our analysis is limited to interactions between moisture

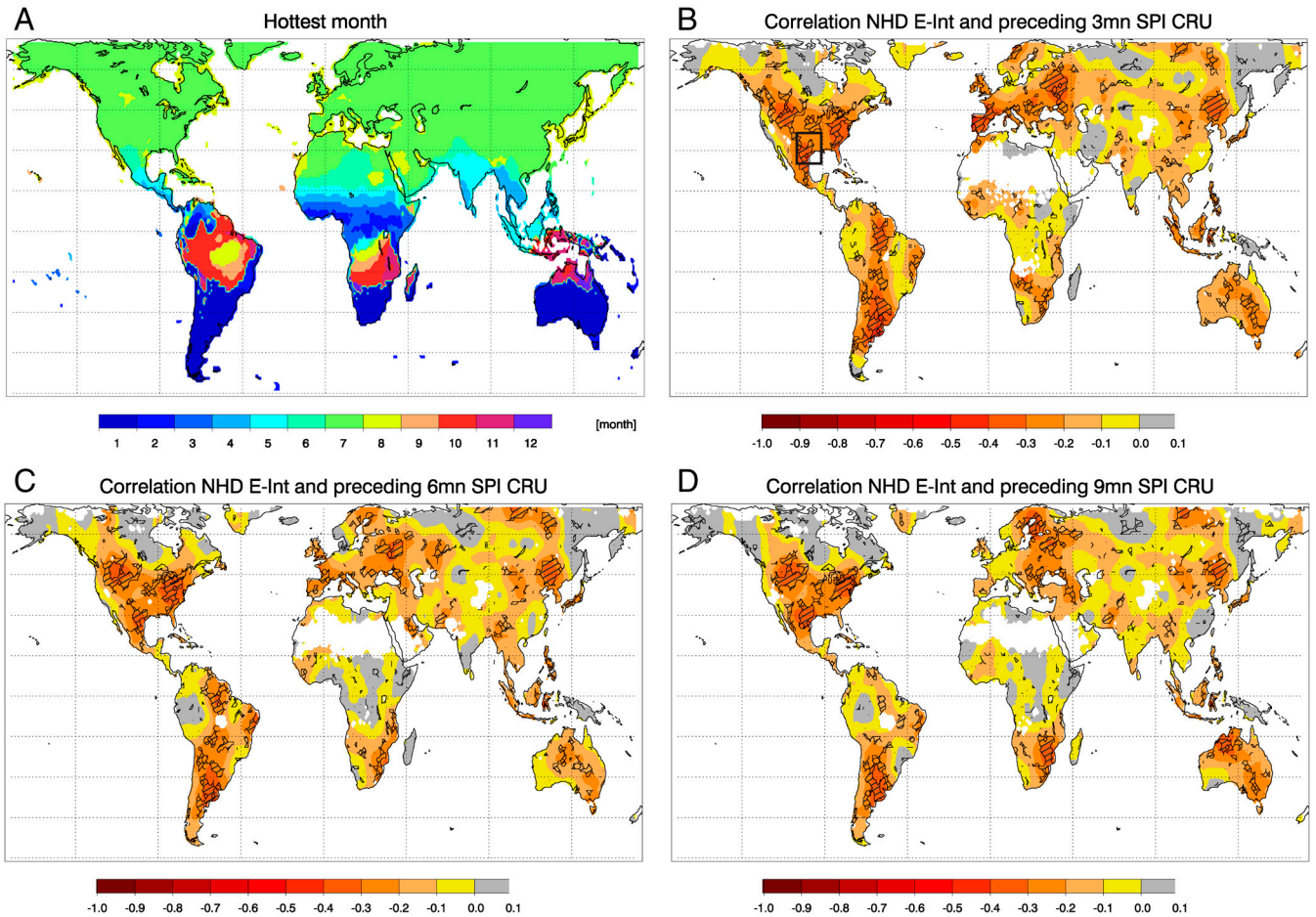

Fig. 1. Relation between number of hot days (NHD) in hottest month of each year and preceding precipitation deficits (SPI). (*A*) Geographical distribution of most frequent hottest month. (*B*) Correlations of NHD in hottest month with 3-month, (*C*) 6-month, and (*D*) 9-month SPI in preceding month. All maps have been smoothed with a boxcar filter of width 10. Significant levels (90%) are not smoothed (hatched). White areas indicate missing values. The employed datasets are ERA-Interim (E-Int) for NHD and CRU for SPI.

deficits and hot extremes, and possible feedbacks with precipitation could be relevant in other regions.

Similar Regions of Strong Coupling Found with Different Observations-Based Datasets. We repeat the analysis of Fig. 1*B* with the NHD calculated from different reanalysis products (Fig. 2 *A* and *C*) and the 3-month SPI from different observations-based precipitation datasets (Fig. 2 *B* and *D*). Using the CFSR or MERRA instead of the ERA-Interim reanalysis for the NHD results in nearly identical regions of strong negative correlations. Using reanalysis data for the NHD seems appropriate since the respective time series agree well with the NHD calculated from an observations-based gridded temperature dataset (see Fig. S1). The choice of the precipitation dataset does also not affect the resulting patterns substantially. Note that the correlations are slightly more consistent for GPCP (Fig. 2*B*) and CPC (Fig. 2*D*) compared to CRU (Fig. 1*B*). A global map of the numbers of dataset combinations with significant correlations is shown in Fig. S2. In addition, we have tested the robustness of our results by changing the choice of months considered for the NHD as well as applying a different hot extreme metric (see Fig. S3).

Quantile Regression Analysis. The slopes of the 10th, 30th, 70th, and 90th quantile regressions of the 3-month SPI (CRU precipitation) with NHD (ERA-Interim temperature) are shown in Fig. 3 *A*–*D*. The patterns of the slopes from the four different quantiles display correspondences in many regions, implying that the SPI generally affects all quantiles of the NHD in the same direction. Furthermore, positive slopes are found to increase towards higher quantiles (from A to D), i.e. higher values of the NHD are more strongly affected by surface wetness conditions than lower values. This also implies that the distribution of the NHD is wider after dry conditions, i.e. both low NHD and very high NHD are found after dry conditions, while wet conditions are strictly followed by a low NHD. This is consistent with previous results for Southeastern Europe (14).

Hot Day Occurrence Probability Larger After Dry than After Wet Conditions. Fig. 4 (*Top*) displays the occurrence probability for an above-average NHD in the hottest month of the year after dry (SPI below −0.8, 4A) and wet (SPI above 0.8, 4B) conditions. The difference between the occurrence probabilities after dry minus wet conditions is displayed in Fig. 4*C*. In many areas, for instance in most parts of the Americas, in Southern and Eastern Europe and Australia, 60 to 80% of the years display an above-average NHD following dry conditions (Fig. 4*A*). The occurrence probability of an extreme NHD (i.e. >150% of average) after dry conditions is 50–60% (see Fig. S4*A*), and the regions correspond very well with those found in Fig. 4. After wet conditions (high SPI), the occurrence probability of an above-average NHD is limited to less than 40% in wide areas (mostly in the same regions, Fig. 4*B*), and extreme NHD (>150%) are very unlikely to occur (probability of less than 20% in many and less than 30% in most areas of the world, Fig. S4*B*). Hence, wet conditions prohibit the occurrence of hot extremes in most regions. Overall, the occurrence probability of an above-average NHD is increased by 30 to 60% after dry compared to wet conditions (Fig. 4*C*) in the regions of strong surface moisture-temperature coupling identified from Fig. 1. These results suggest that effects of soil moisture conditions on the occurrence probability of hot days are relevant in a

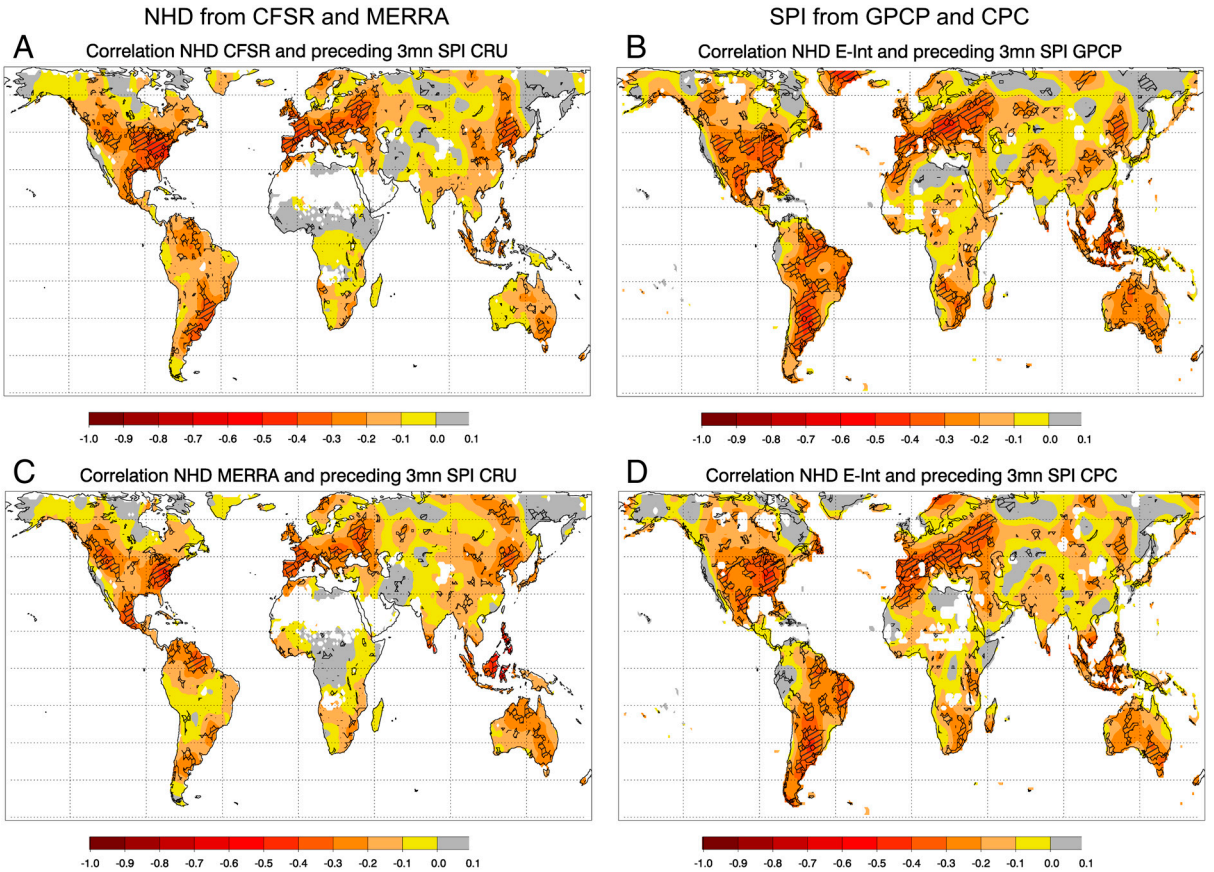

Fig. 2. Relation between number of hot days (NHD) in hottest month of each year and preceding 3-month precipitation deficits (SPI) for different reanalysis datasets (NHD, *A* and *C*), and different precipitation datasets (SPI, *B* and *D*). (*A*) CFSR NHD correlated with CRU SPI, (*B*) ERA-Interim NHD with GPCP SPI, (*C*) MERRA NHD with CRU SPI, and (*D*) ERA-Interim NHD with CPC SPI. Significant levels (90%) are not smoothed (hatched). White areas indicate missing values.

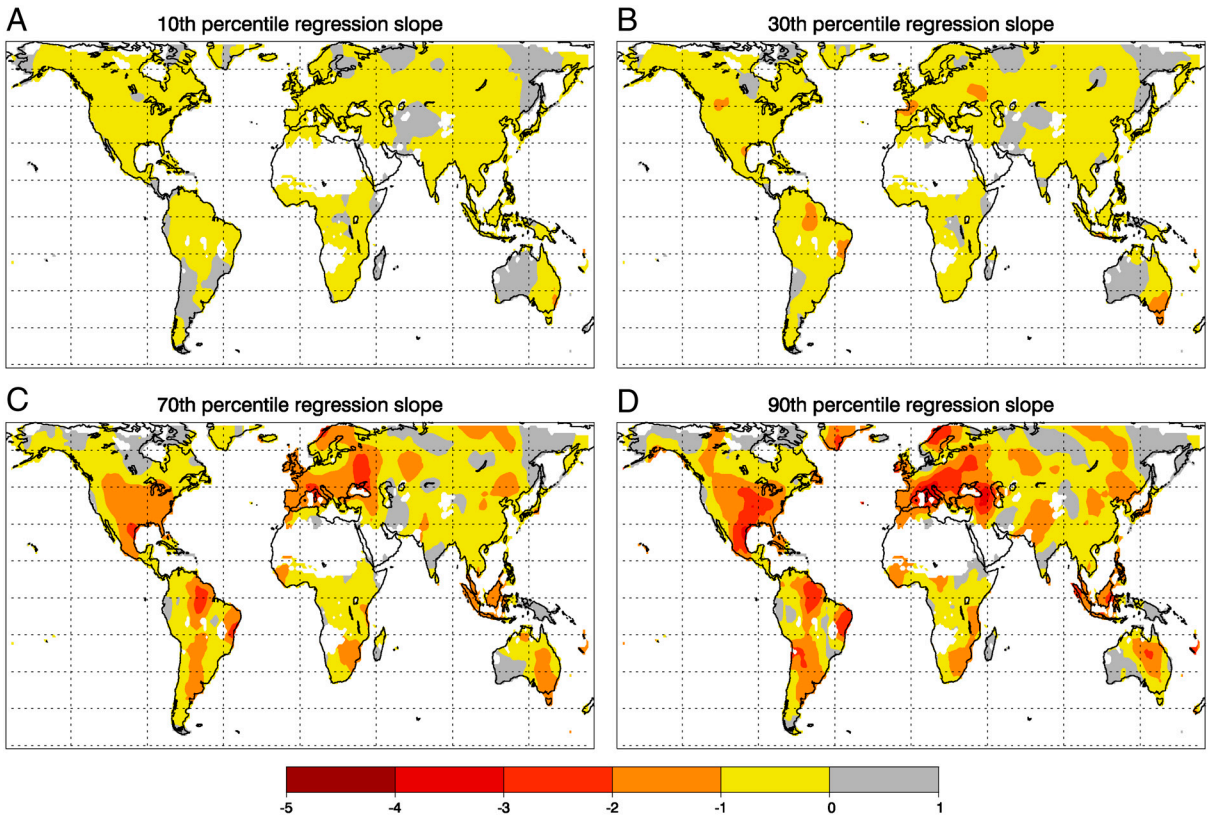

Fig. 3. Quantile regression of NHD in hottest month of each year and preceding 3-month SPI. Slope of regression lines of 10th (*A*), 30th (*B*), 70th (*C*) and 90th (*D*) percentiles. White areas indicate missing values. The employed datasets are ERA-Interim for NHD and CRU for SPI.

large fraction of the globe. This has important implications for the improvement of forecasting skill of hot extremes in these regions.

Texas Conditions Illustrate Asymmetrical Impact. We illustrate the asymmetrical impact of the SPI on the NHD at the example of Texas (region indicated in Fig. 1*B*), which was hit by an exceptional drought and heat wave in the 2011 summer. In order to include data from the 2011 summer in this analysis, ERA-Interim instead of CRU precipitation is used to calculate the SPI statistics. A comparison of the SPI calculated from the two different datasets reveals a close correspondence between the two products (Fig. S5). As identified from Fig. 3 *A–D* for the above-highlighted regions, the slopes of the quantile regressions also increase towards higher percentiles in Texas, and the conditions of the 2011 summer fit well in the overall distributions (Fig. 5*A*). Consistent with the results from Fig. 3, the relative frequency distribution of the NHD (Fig. 5*B*) is narrower for wet (SPI above 0.8) and wider for dry (SPI below −0.8) years, and the analysis indicates that the high tails of the NHD distribution are more strongly influenced by precipitation (and soil water) deficits.

Conclusions

Our observational analysis suggests a strong relationship between precipitation deficits and the subsequent occurrence of hot extremes in a large fraction of the world, such as most areas of North and South America, Europe, Australia and parts of China. The correlation of the precipitation deficits is found to be strongest with high compared to low extremes of hot day occurrences. Correspondingly, the occurrence probability of an above-average number of hot days is high after dry conditions and low after wet conditions in the identified regions. It is noteworthy that we find several additional regions of strong soil moisture-atmosphere coupling in comparison to previous studies that were based on model data only (21, 29).

In summary, our results show that surface moisture deficits are a relevant factor for the occurrence of hot extremes in many areas of the world. This suggests that hot day predictions could be substantially improved in operational forecasts in these regions with the aid of soil moisture initialization. This would allow the development of early warning and adaptation measures previous to the occurrence of hot extremes, not only in regions typically referred to as hot spots of land-atmosphere coupling (e.g. North American Great Plains) (21), but also in several additional regions such as the European continent, and a large fraction of the Southern Hemisphere.

Materials and Methods

CRU 3.1 precipitation data (30) have been used to calculate the SPI for the main analyses. SPI has also been calculated from GPCP (31), CPC (32) and the atmospheric reanalysis ERA-Interim (27) (only used in Fig. 5 and Fig. S5) precipitation data. The reference period for the CRU SPI is 1950–2009, for the GPCP SPI 1979–2010, for the CPC SPI 1979–2009 and for the ERA-Interim SPI 1979–2011. The reference period for all NHD calculations is 1979–2010 (except for Fig. S5, where it is 1979–2011). Information on the atmospheric reanalyses MERRA and CFSR can be found in the literature (33, 34). E-Obs maximum temperature values (35) are employed for the verification of reanalyses based NHD in Fig. S1. For the normalization of the precipitation data with the gamma distribution that is needed to compute the SPI, the goodness of fit was tested using the critical values of the Kolmogorov-Smirnov test. All analyses have only been performed when the goodness of fit test was significant at the 5%-level. SPI and NHD data were linearly interpolated on a $1° \times 1°$ resolution. All maps have been smoothed with a boxcar filter of width 10 (width 3 for Fig. S2) to enhance readability. The significance of the correlations have been estimated with a *t*-Test (90%-level) and have not been smoothed.

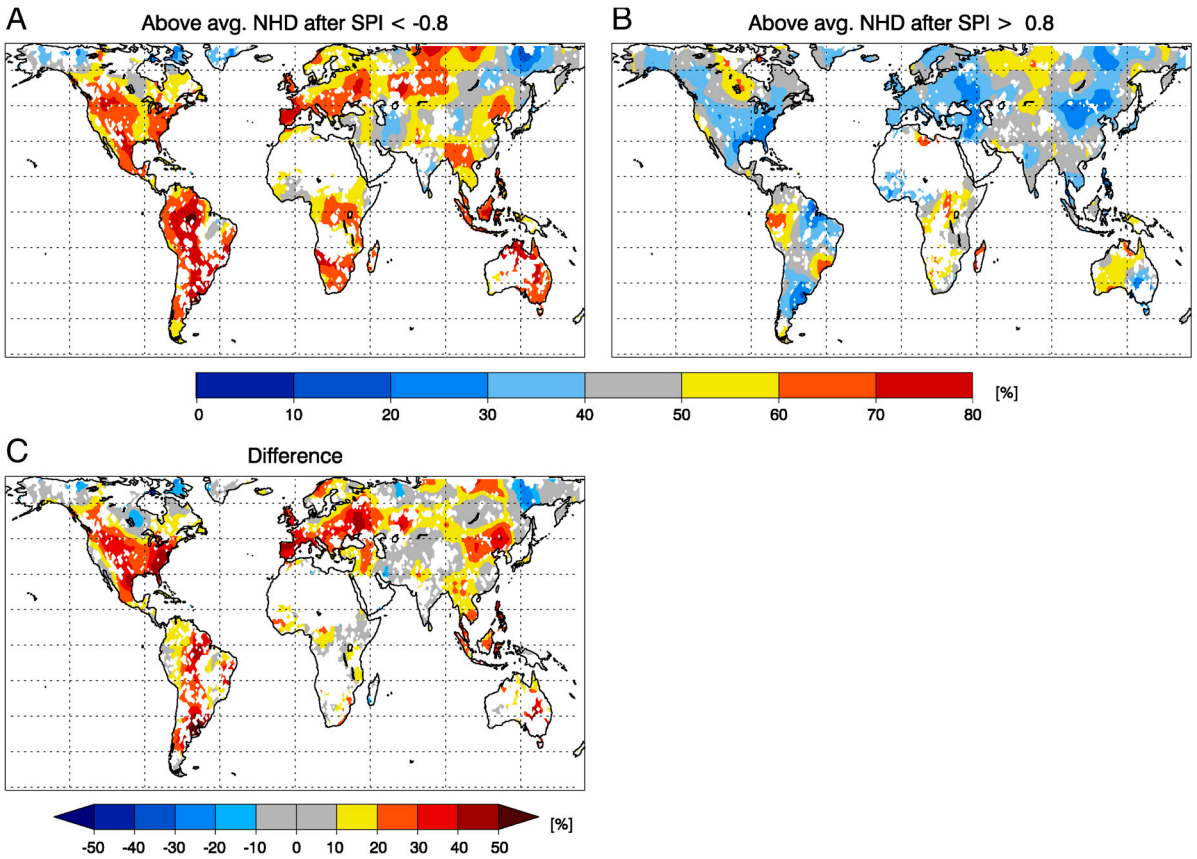

Fig. 4. Hot day occurrence probability after dry versus wet conditions. Occurrence probability for above-average number of hot days in the respective hottest month of each year following low 3-month SPI values (dry conditions, *A*) and high 3-month SPI values (wet conditions, *B*), and difference between the two (*C*). Values are given in percentage of years with above-average NHD from total number of low and high SPI years, respectively. Values that are based on a composite of less than 4 years are not shown (white areas). The employed datasets are ERA-Interim for NHD and CRU for SPI.

ACKNOWLEDGMENTS. CRU data were obtained from the University of East Anglia Climate Research Unit (CRU), British Atmospheric Data Centre, 2008, available from http://badc.nerc.ac.uk/data/cru. The GPCP combined precipitation data were developed and computed by the NASA/Goddard Space Flight Center's Laboratory for Atmospheres as a contribution to the GEWEX Global Precipitation Climatology Project. CPC merged analysis of precipitation data were provided by the NOAA/OAR/ESRL PSD, Boulder, Colorado, USA, from their Web site at http://www.esrl.noaa.gov/psd/. We acknowledge the Global Modeling and Assimilation Office and the GES DISC for the dissemination of MERRA, and the ECMWF for the dissemination of ERA-Interim data. The CFSR data are from the Research Data Archive which is maintained by the Computational and Information Systems Laboratory at the National Center for Atmospheric Research (NCAR). NCAR is sponsored by the National Science Foundation. The original data are available from the RDA

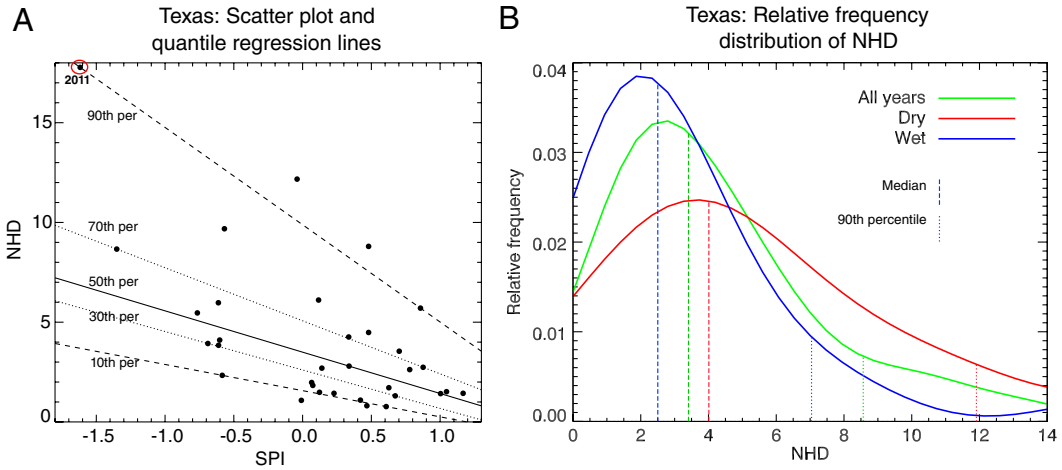

Fig. 5. Quantile regression analysis and relative frequency distribution for Texas. (*A*) Scatter plots of ERA-Interim NHD in hottest month of respective year and 3-month SPI in preceding month averaged over Texas region (black square in Fig. 1*B*) with regression slopes (10th, 30th, 50th, 70th, and 90th percentiles) as an example for a region with strong coupling as defined in Fig. 1. The SPI in (*A*) is calculated from ERA-Interim precipitation data (includes 2011, indicated with a circle). (*B*) Relative frequency distribution of NHD for all, dry and wet years, including indication of median (3 vertical dashed lines) and 90th percentile values (3 vertical dotted lines).

(http://dss.ucar.edu) in dataset number ds093.0. We thank Martin Hirschi and Jan Sedlacek for useful discussions. We also thank two anonymous reviewers for helpful comments on the manuscript. We acknowledge partial financial support from the EU-FP7 DROUGHT-RSPI and EU-FP7 EMBRACE projects.

1. Easterling DR, et al. (2000) Climate extremes: Observations, modeling, and impacts. *Science* 289:2068–2074.
2. Sherwood SC, Huber M (2010) An adaptability limit to climate change due to heat stress. *Proc Natl Acad Sci USA* 107:9552–9555.
3. Anderson GB, Bell ML (2011) Heat waves in the United States: Mortality risk during heat waves and effect modification by heat wave characteristics in 43 U.S. communities. *Environ Health Persp* 119:210–218.
4. IPCC (2012) Summary for policymakers. *Intergovernmental Panel on Climate Change Special Report on Managing the Risks of Extreme Events and Disasters to Advance Climate Change Adaptation*, eds CB Field et al. (Cambridge University Press, Cambridge, UK and New York, NY), pp 1–19.
5. Klein Tank AMG, et al. (2006) Changes in daily temperature and precipitation extremes in central and south Asia. *J Geophys Res-Atmos* 111:D16105.
6. Alexander LV, et al. (2006) Global observed changes in daily climate extremes of temperature and precipitation. *J Geophys Res-Atmos* 111:D05109, doi: 10.1029/2005JD006290.
7. Tebaldi C, Hayhoe K, Arblaster JM, Meehl GA (2006) Going to the extremes. *Clim Change* 79:185–211.
8. Meehl G, et al. (2007) Global climate projections. *Clim Change 2007: The Physical Science Basis*, eds S Solomon et al. (Cambridge University Press, Cambridge, UK and New York, NY).
9. Orlowsky B, Seneviratne SI (2012) Global changes in extreme events: regional and seasonal dimension. *Clim Change* 110:669–696.
10. Seneviratne SI, et al. (2010) Investigating soil moisture-climate interactions in a changing climate: A review. *Earth Sci Rev* 99:125–161.
11. Durre I, Wallace JM, Lettenmaier DP (2000) Dependence of extreme daily maximum temperatures on antecedent soil moisture in the contiguous United States during summer. *J Clim* 13:2641–2651, doi: 10.1175/1520-0442(2000)013-2641:DOEDMT-2.0.CO;2.
12. Fischer EM, Seneviratne SI, Vidale PL, Luthi D, Schar C (2007) Soil moisture—atmosphere interactions during the 2003 European summer heat wave. *J Clim* 20:5081–5099.
13. Della-Marta PM, et al. (2007) Summer heat waves over western Europe 1880–2003, their relationship to large-scale forcings and predictability. *Clim Dynam* 29:251–275.
14. Hirschi M, et al. (2011) Observational evidence for soil-moisture impact on hot extremes in southeastern Europe. *Nat Geosci* 4:17–21, doi: 10.1038/NGEO1032.
15. Seneviratne SI, Lüthi D, Litschi M, Schär C (2006) Land-atmosphere coupling and climate change in Europe. *Nature* 443:205–209.
16. Diffenbaugh NS, Pal JS, Giorgi F, Gao XJ (2007) Heat stress intensification in the Mediterranean climate change hotspot. *Geophys Res Lett* 34:L11706.
17. Alexander L (2011) Extreme heat rooted in dry soils. *Nat Geosci* 4:12–13, doi: 10.1038/ngeo1045.
18. Vautard R, et al. (2007) Summertime European heat and drought waves induced by wintertime mediterranean rainfall deficit. *Geophys Res Lett* 34:L07711.
19. Haarsma RJ, Selten F, Hurk BV, Hazeleger W, Wang XL (2009) Drier mediterranean soils due to greenhouse warming bring easterly winds over summertime Central Europe. *Geophys Res Lett* 36:L04705.
20. Lorenz R, Jaeger EB, Seneviratne SI (2010) Persistence of heat waves and its link to soil moisture memory. *Geophys Res Lett* 37:L09703, doi: 10.1029/2010GL042764.
21. Koster RD, et al. (2004) Regions of strong coupling between soil moisture and precipitation. *Science* 305:1138–1140.
22. McKee T, Doesken N, Kleist J (1993) The relationship of drought frequency and duration to time scales. *8th Conference on Applied Climatology* pp 179–184.
23. Koenker R, Bassett GW (1978) Regression quantiles. *Econometrica* 46:33–50.
24. Koenker R (2005) Quantile regression (Econometric Society Monographs). *Econometric Society Monographs*, (Cambridge University Press, New York), Vol 38.
25. Owe M, de Jeu R, Walker J (2001) A methodology for surface soil moisture and vegetation optical depth retrieval using the microwave polarization difference index. *IEEE Trans Geosci Remote Sens* 39:1643–1654.
26. Zhang X, et al. (2011) Indices for monitoring changes in extremes based on daily temperature and precipitation data. *WIREs Clim Change* 2:851–870.
27. Dee DP, et al. (2011) The ERA-Interim reanalysis: Configuration and performance of the data assimilation system. *Quat J Roy Meteorol Soc* 137:553–597.
28. Koster RD, et al. (2011) The second phase of the global land-atmosphere coupling experiment: Soil moisture contributions to subseasonal forecast skill. *J Hydrometeorol* 12:805–822.
29. Dirmeyer PA (2011) The terrestrial segment of soil moisture-climate coupling. *Geophys Res Lett* 38:L16702.
30. Mitchell TD, Jones PD (2005) An improved method of constructing a database of monthly climate observations and associated high-resolution grids. *Int J Climatol* 25:693–712.
31. Adler RF, et al. (2003) The version-2 global precipitation climatology project (GPCP) monthly precipitation analysis (1979-present). *J Hydrometeorol* 4:1147–1167.
32. Huffman GJ, et al. (1997) The global precipitation climatology project (GPCP) combined precipitation dataset. *Bull Am Meteorol Soc* 78:5–20.
33. Rienecker MM, et al. (2011) MERRA: Nasa's modern-era retrospective analysis for research and applications. *J Clim* 24:3624–3648.
34. Saha S, et al. (2010) The NCEP climate forecast system reanalysis. *Bull Am Meteorol Soc* 91:1015–1057.
35. Haylock MR, et al. (2008) A European daily high-resolution gridded data set of surface temperature and precipitation for 1950–2006. *J Geophys Res-Atmos* 113:D20119.